

ActVAR: Activating Mixtures of Weights and Tokens for Efficient Visual Autoregressive Generation

Kaixin Zhang¹, Ruiqing Yang², Yuan Zhang³, Shan You⁴, Tao Huang^{5*}

¹School of Computer Science and Engineering, Central South University,

²University of Electronic Science and Technology of China,

³School of Computer Science, Peking University,

⁴SenseTime Research, ⁵Shanghai Jiao Tong University

kaixinzhang@csu.edu.cn, yrq@std.uestc.edu.cn,

zhangyuan@alumni.pku.edu.cn, youshan@sensetime.com, t.huang@sjtu.edu.cn

Abstract

Visual Autoregressive (VAR) models enable efficient image generation via next-scale prediction but face escalating computational costs as sequence length grows. Existing static pruning methods degrade performance by permanently removing weights or tokens, disrupting pretrained dependencies. To address this, we propose ActVAR, a dynamic activation framework that introduces dual sparsity across model weights and token sequences to enhance efficiency without sacrificing capacity. ActVAR decomposes feedforward networks (FFNs) into lightweight expert sub-networks and employs a learnable router to dynamically select token-specific expert subsets based on content. Simultaneously, a gated token selector identifies high-update-potential tokens for computation while reconstructing unselected tokens to preserve global context and sequence alignment. Training employs a two-stage knowledge distillation strategy, where the original VAR model supervises the learning of routing and gating policies to align with pre-trained knowledge. Experiments on the ImageNet 256×256 benchmark demonstrate that ActVAR achieves up to 21.2% FLOPs reduction with minimal performance degradation.

1. Introduction

Autoregressive models, which predict the next token based on preceding ones, have demonstrated remarkable success in image generation [9, 25, 37]. LLaMAGen [32] redesigns the tokenizer to support variable downsampling ratios, further improving image generation quality. Despite these advances, such methods remain limited by the standard next-token prediction paradigm, which typically requires a large

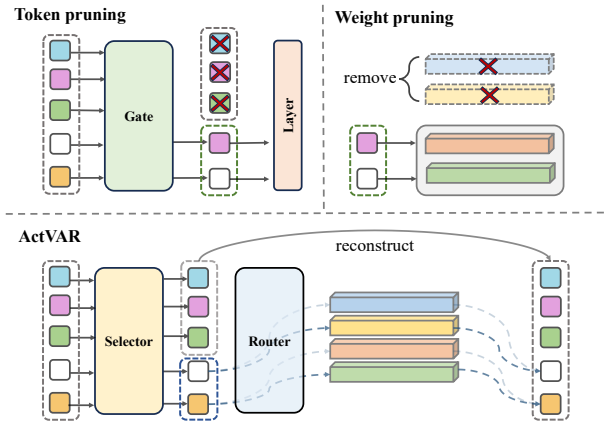


Figure 1. **Comparisons of conventional weight and token pruning methods and our proposed ActVAR.** Conventional methods permanently remove the weights and tokens, disrupting the dependencies. Our ActVAR achieves the same efficiency without sacrificing capacity.

number of generation steps and leads to slow inference.

Recently, VAR [34] innovatively proposes the next-scale prediction paradigm, effectively enhancing image quality and generation speed. However, the VAR-based methods [12, 33] approach introduces intermediate-scale features, which expand the sequence length and incur considerable computational cost.

A straightforward approach to reducing the computational cost of VAR models is to apply conventional weight and token pruning techniques for transformers (*e.g.*, ToMe [2] for ViT, and SparseVLM [43] for VLM). However, our empirical analysis reveals that such methods are only effective under low compression ratios¹. We hypothe-

*Corresponding author

¹FastVAR yields merely the 8% reduction in inference time on 256×256 image generation, at the cost of increasing the FID from 2.29 to 2.64.

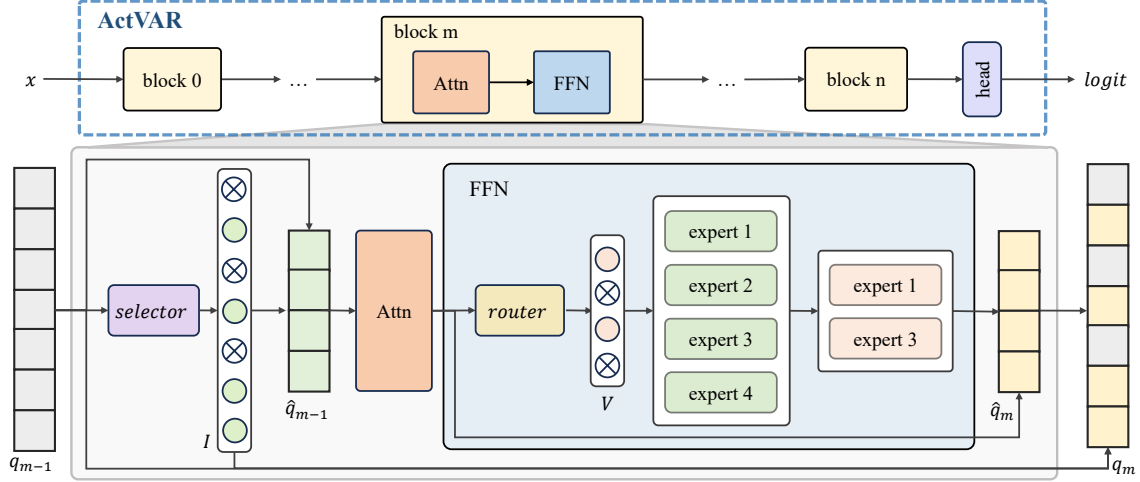


Figure 2. **The pipeline of our ActVAR.** For the input sequence q_{m-1} , the selector generates a binary indicator vector I . Based on I , a filtered input \hat{q}_{m-1} is constructed and passed through the attention and FFN layers. In the FFN, the router assigns each token to a subset of experts by predicting expert activation probabilities. Finally, the output \hat{q}_m is reconstructed into the complete sequence q_m using the indicator vector I , maintaining alignment with the original scale.

size that this limitation stems from the teacher-forcing training strategy employed in VAR, which makes the model particularly sensitive to structural changes. As illustrated in Figure 1, the permanent removal of weights and tokens disrupts the learned dependencies and amplifies error accumulation during generation, ultimately degrading output quality. This motivates a key idea: *can we dynamically activate only important weights and tokens at each layer, while keeping the rest unchanged, so that the model retains its full representational capacity and avoids information loss?*

In this paper, inspired by mixture-of-experts methods [4, 48], we propose Activation VAR (ActVAR), a novel framework that introduces dual sparsity across both weights and tokens, as shown in Figure 2. Specifically, we treat subsets of weights and tokens as experts, and dynamically activate only the most relevant subsets for each token and each layer. To achieve this, ActVAR decomposes the FFN into multiple sub-network experts and employs a learnable router to select token-specific expert combinations. To further reduce computation for long sequences, we introduce a gated token selector, which learns to identify and retain only the most up-to-date worthy tokens for each processing block. Crucially, unselected tokens are not discarded but incorporated into a lightweight reconstruction step that still preserves global context and sequence alignment for next-token prediction.

For training ActVAR, we design a two-stage training strategy inspired by knowledge distillation [14], where a pre-trained VAR model acts as the teacher to supervise both the router and the selector. In the first stage, we train the router and gated token selector to adaptively assign experts and select informative tokens based on input semantics. In

the second stage, we fine-tune the generative model to align with the learned routing and gating policies, while applying distillation losses to effectively transfer knowledge from the teacher model to ActVAR models.

In summary, the contributions of our work are as follows:

- We propose **ActVAR**, a novel dynamic computation framework for autoregressive image generation that preserves the full model capacity while reducing inference overhead. Instead of permanently pruning weights or tokens, ActVAR selectively **activates** them at inference time based on input content, avoiding information loss and maintaining output quality.
- ActVAR introduces two lightweight routing modules: a *weight router* that dynamically selects a subset of FFN sub-experts for each token, and a *token router* that identifies important tokens to undergo further computation. This joint routing mechanism allows the model to adaptively allocate computational resources where needed.
- We conduct comprehensive experiments on the ImageNet 256×256 benchmark, demonstrating that ActVAR achieves up to 21.2% FLOPs saving with minimal performance drop.

2. Related Work

2.1. Autoregressive Models in Image Generation

Prior works [17, 26, 29, 47] introduce the next-pixel prediction paradigm, which adapts NLP-style token modeling to images by treating pixels as tokens. For example, some approaches [5, 6, 36] typically flatten the two-dimensional image into a one-dimensional sequence using raster scan order, then employ CNNs or transformers to predict each

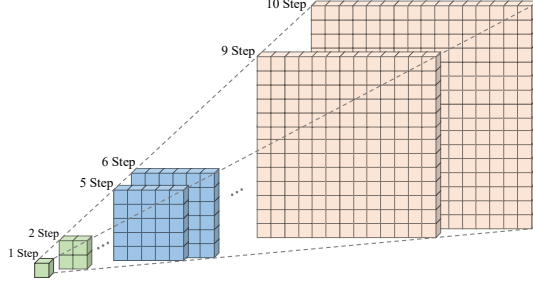


Figure 3. The number of tokens generated by VAR models at each step is increasing rapidly.

pixel based on its predecessors. Subsequently, the tokenizer [9, 37] is introduced to compress continuous images into discrete tokens and use a transformer decoder to predict these tokens. Building upon this pipeline, many studies [22, 32, 39, 49] achieve performance on par with advanced diffusion models [23, 24, 27]. However, the next-token prediction paradigm inherently requires a large number of decoding steps, which limits the overall efficiency of image generation. To address this, VAR [34] recently proposed the next-scale prediction paradigm, which significantly reduces the number of generation steps and offers a promising direction for improving the efficiency of autoregressive models.

2.2. Acceleration of Autoregressive Models

Transformer [38] has become a mainstream architecture in both natural language processing [3, 7] and computer vision [8, 20, 35], largely due to their scalability and strong performance. However, this performance comes at the cost of substantial computational overhead, resulting in high resource demands for full-scale deployment. To address this issue, many studies [21, 30, 42, 50] have proposed sophisticated techniques aimed at reducing model redundancy and accelerating inference. Inspired by the above studies, some efforts [13, 19, 32] focus on accelerating transformer-based autoregressive models. For example, the work [31] introduces structural weight pruning to compress the decoder-only transformer. Another study [1] proposes a novel context pruning method to remove redundant tokens from the token sequence. Although VAR offers a promising alternative for efficient image generation, research on optimizing its computational performance remains scarce [11, 40]. This work aims to bridge that gap by investigating weights and token activation strategies tailored to VAR.

3. Proposed Approach: ActVAR

3.1. Computation Analysis of VAR

Visual autoregressive (VAR) modeling introduces the innovative next-scale prediction paradigm, which replaces tradi-

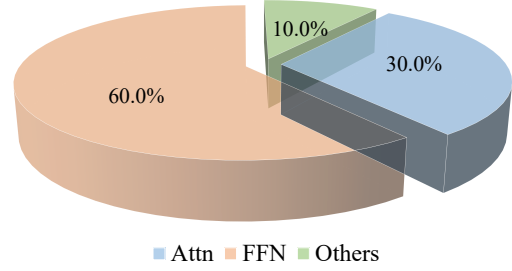


Figure 4. Distribution of computation per transformer block in VAR models.

tional token-by-token generation with the prediction of entire token maps at different scales. Given an image feature map $I \in \mathbb{R}^{H \times W \times C}$, VAR quantizes it into a set of multi-scale token maps $R = [r_1, r_2, \dots, r_N]$. A transformer model is then used in an autoregressive manner to predict all token maps sequentially from small to large scales:

$$p(r_1, r_2, \dots, r_N) = \prod_{i=1}^N p(r_i | r_1, r_2, \dots, r_{i-1}), \quad (1)$$

where the initial token r_1 is a class-condition embedding, and N denotes the number of scales in total.

During inference, VAR takes the interpolated upsampling of the last scale as input to predict all tokens at the next scale. This approach reduces the number of inference steps compared to vanilla autoregressive models. However, as shown in Figure 3, VAR still suffers from long input sequences at large scales, resulting in increased computational overhead. For instance, VAR requires a token sequence of length 680 to generate a 256×256 image, compared to only 256 tokens in standard AR methods. As image resolution or generation granularity increases, this discrepancy in sequence length introduces substantial computational overhead, which severely constrains the scalability of vanilla VAR.

To reduce the computational cost of VAR while keeping the generation capability as much as possible, we propose to dynamically activate only valuable computations and reduce the unnecessary computations as much as possible.

We begin by analyzing the computational costs of different modules in the VAR model. As shown in Figure 4, most of the computations are introduced by the feedforward networks (FFNs) and attention layers. Besides, it is acknowledged that the FFNs are computationally expensive due to the high-dimensional dense projections, while the attention computation is proportional to the sequence length. As a result, to reduce both the computational costs of FFNs and attentions, we should consider reducing both the dimensions of FFNs and the sequence length of visual tokens.

As a result, we introduce ActVAR, a method to dynamically activate important weights and tokens. We will offi-



Figure 5. **Visualization of dynamic weight activations.** The FFN is partitioned into 16 expert networks. At a 16×16 scale, the above four images show the top-3 expert networks for all token activations in different steps. Notably, the activation patterns vary significantly across steps, as tokens at different steps exhibit distinct preferences in their activation weights.

cially introduce our method as follows.

3.2. FFN as Mixture of Experts

The most direct way to improve the computational efficiency of FFNs is weight pruning. However, this method sacrifices model capacity and disrupts the original network structure. A more effective alternative is to retain the full set of weights and dynamically activate a subset based on the properties of the input during inference. As illustrated in Figure 5, the preference activation weights dynamically change across steps while generating an image.

The linear layer, weighted by $W \in \mathbb{R}^{d_1 \times d_2}$, can be regarded as the summation of d_1 matrix computations, *i.e.*,

$$xW = \sum_i^{d_1} x_i W_i. \quad (2)$$

This reminds us of mixture-of-experts (MoEs) [45, 46], which adaptively select K out of N experts based on the input features. Therefore, we can use the idea of MoEs to selectively activate only a subset of FFN weights. Now we discuss the formal method for activating FFN weights as a mixture of experts.

Weight decomposition. The FFN module is implemented as a two-layer fully connected network. Given an input token x , the transformation process within the module can be described as follows:

$$\begin{aligned} h &= xW_1 + b_1, \\ F(x) &= \delta(h)W_2 + b_2, \end{aligned} \quad (3)$$

where $W_1 \in \mathbb{R}^{d_p \times d_h}$ and $b_1 \in \mathbb{R}^{d_h}$ are the weights and biases of the first linear layer, and $W_2 \in \mathbb{R}^{d_h \times d_p}$ and $b_2 \in \mathbb{R}^{d_p}$ correspond to those of the second layer. The function $\delta(\cdot)$ denotes the activation function *GELU*.

In the construction of the expert networks, we divide the FFN into N equally sized sub-networks. This design not

only mitigates potential capacity bottlenecks but also eliminates latency issues that could arise from heterogeneous sub-network structures during parallel computation.

Specifically, for a complete FFN, the decomposed parameters can be expressed as $W_1^i \in \mathbb{R}^{d_p \times d_e}$ and $W_2^i \in \mathbb{R}^{d_e \times d_p}$ for the weights, and $b_1^i \in \mathbb{R}^{d_e}$ for the biases, where the dimensionality of each sub-network satisfies $d_e = d_h/N$. Note that, according to the rules of matrix computation, the bias term b_2 remains unchanged.

Dynamic activation of weights. The routing mechanism is designed to adaptively assign a suitable expert network based on the characteristics of each input token. Specifically, for a given token x , the router $R(\cdot)$ computes the assignment probability $p_w \in \mathbb{R}^N$ for each expert network. The top- k function is applied to p_w to obtain the indicator vector $\mathcal{V} \in \{0, 1\}^N$ corresponding to the activated experts.

Based on the indicator vector, mapping rules are defined to construct the corresponding set of activated experts $\mathcal{E} = \{e^j\}_{j=1}^{K_w}$. Therefore, the final output of the dynamically activated experts can be formulated as the sum of the outputs from all selected experts:

$$\sum_{j \in \mathcal{E}} e^j(x) = \sum_{j \in \mathcal{E}} \left(\delta(xW_1^j + b_1^j)W_2^j + b_2 \right), \quad (4)$$

where W_1^j and W_2^j are the weights of the j -th expert. b_1^j is the bias for the first layer, and b_2 is the shared bias term for the second layer.

Optimize dynamic router. Since the routing module lacks soft supervision, we need to construct an extra training signal. Inspired by knowledge distillation [14, 16, 44], we treat the original feedforward network F_θ as a teacher model, which incorporates comprehensive pre-trained knowledge and capabilities. Here, the expert networks $\mathcal{E}_\theta = \{e^i\}_{i=1}^N$ are regarded as a group of student models. For each expert, we compute the mean squared error (MSE) between its output and that of the teacher, yield-

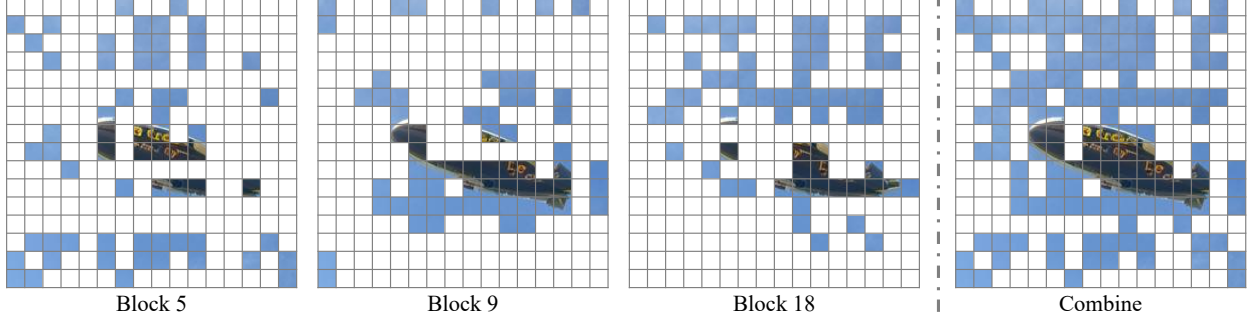


Figure 6. **Visualization of dynamic token activations.** The first three images on the left illustrate that, at a 16×16 scale, each block dynamically activates tokens at distinct spatial positions. The image on the right aggregates the activation maps from the preceding three, highlighting the overall distribution of token activations.

ing a distance vector $\{d_i^w\}_{i=1}^N$. The distance is intended to quantify the divergence between the expert output and the teacher output. Therefore, a top- k selection based on the distances is performed to identify the most relevant experts and yields a pseudo-label matrix:

$$\mathcal{A}_w = \sigma(\text{top} - k(\{-d_i^w\}_{i=1}^N, K_w)), \quad (5)$$

where $\sigma(\cdot)$ denotes the softmax function. Under the supervision of the pseudo-label matrix \mathcal{A}_w , we employ a distillation loss to encourage the routing module $R(\cdot)$ to align its predicted probabilities p_w with the softened \mathcal{A}_w :

$$L_{dis}^w = \text{KL}(p_w \parallel \sigma(\mathcal{A}_w)) = \sum_{i=1}^N p_w \log \frac{p_w}{\sigma(\mathcal{A}_w)}, \quad (6)$$

where $\text{KL}(\cdot)$ is the Kullback–Leibler divergence.

Furthermore, MoE-based architectures often suffer from load imbalance and degraded performance due to over-reliance on a small subset of experts [10]. To mitigate this issue, we follow [18] and incorporate a load balancing loss that penalizes the uneven distribution of input tokens across experts:

$$L_{bl} = \frac{K_w}{N} \sum_{i=1}^N \sum_{j=1}^{K_w} \mathbb{I}_j(x_i) R_j(x_i), \quad (7)$$

where x_i denotes the i -th token in the input sequence. The indicator function $\mathbb{I}_j(x_i)$ equals 1 if the j -th expert is selected to process x_i via the top- K routing mechanism, and 0 otherwise. In this way, the routing mechanism can learn to mimic the implicit preference of the teacher model for expert specialization.

3.3. Layer-Adaptive Token Activation

In addition to improving efficiency at the weight level, adaptively selecting tokens can further reduce the computational burden of VAR models, which would otherwise need to process long token sequences. As illustrated in Figure 6, unlike

static token pruning methods, our layer-adaptive token activation retains all tokens throughout the model. At each transformer block, we dynamically select a subset of tokens with the highest optimization potential to participate in the computation, effectively reducing the overall computational cost of the model.

Unselected tokens are not discarded. Instead, they are reconsidered in subsequent layers, allowing for broader and more flexible coverage across the entire sequence. This ensures that most tokens have opportunities to be optimized at different layers. Since these unselected tokens still contain rich positional and contextual information, we reuse them to reconstruct the complete token sequence. This reconstruction preserves input-output alignment and maintains the original spatial structure of all tokens.

Adaptive token activation. For the input token sequence $q_{m-1} \in \mathbb{R}^L$ of the transformer block m , a lightweight gated selector $G(\cdot)$ is trained to predict the probabilities $p_s \in \mathbb{R}^L$ that tokens are likely to undergo significant updates in the block. We then utilize the top- k function to obtain the indicator matrix $\mathcal{I} = \{0, 1\} \in \mathbb{R}^L$ representing the activations of the tokens. Depending on this indicator matrix, we extract the corresponding tokens from q_{m-1} to form a compact sequence $\hat{q}_{m-1} \in \mathbb{R}^{K_t}$, which is then passed through the Attention and FFN module:

$$\hat{q}_m = \text{FFN}(\text{Attn}(\hat{q}_{m-1})), \quad (8)$$

where $\hat{q}_m \in \mathbb{R}^{K_t}$ denotes the updated sequence, and K_t is the number of selected token.

To reconstruct the complete output sequence $q_m \in \mathbb{R}^L$, we map the updated sequence \hat{q}_m into their original positions in q_{m-1} based on the indicator matrix \mathcal{I} . The reconstruction process is defined as:

$$q_m^i = \begin{cases} \hat{q}_m^i, & \text{if } \mathcal{I}_t^i = 1, \\ q_{m-1}^i, & \text{otherwise,} \end{cases} \quad (9)$$

where \mathcal{I}^i represents that the i -th position reuses the input token. This design enables complete knowledge reuse and

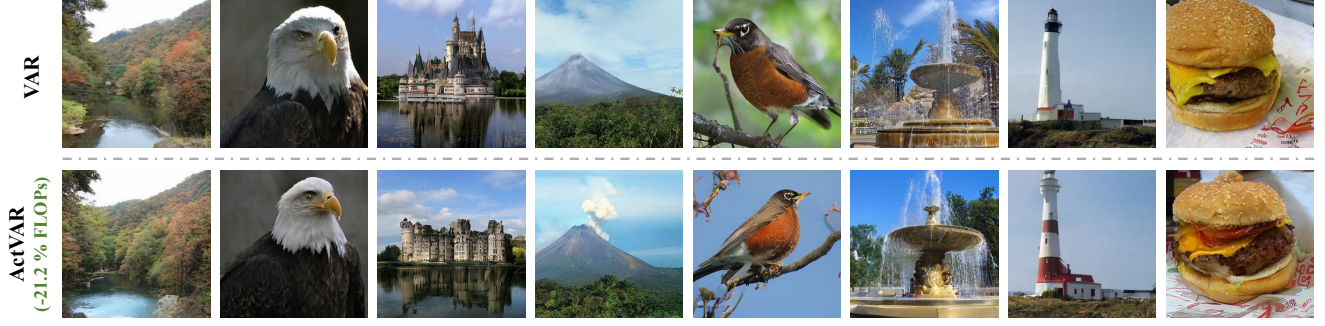


Figure 7. Comparison between the original VAR and our proposed ActVAR on 256×256 image generation.

preserves dimensional consistency between the input and output in VAR models.

Optimize gated selector. To simplify our method, when training the selector $G(\cdot)$, we adopt an optimization scheme similar to that used for training the router. We pass the entire input sequence q_{m-1} through the transformer block to obtain a fully updated sequence q_m^* . We then measure the token-wise distance $\{d_i^t\}_{i=1}^M$ between q_{m-1} and q_m^* to quantify how much each token changes during the update. Tokens exhibiting larger variations are regarded as carrying higher optimization potential. Guided by this metric, we employ the top- k function to identify valuable tokens and construct a pseudo-label matrix \mathcal{A}_t for gate training:

$$\mathcal{A}_t = \sigma(\text{top} - k(\{d_i^t\}_{i=1}^M, K_t)), \quad (10)$$

where M denotes the number of tokens in the input sequence.

Guided by the pseudo-label matrix \mathcal{A}_t , the $G(\cdot)$ is trained using a distillation loss, which enforces consistency between its predicted token selections and the target patterns:

$$L_{dis}^t = \text{KL}(p_t \parallel \sigma(\mathcal{A}_t)). \quad (11)$$

Furthermore, we employ the same load balancing loss to penalize the uneven activations among the experts. The details of our two-stage training strategy are provided in the Supplementary Materials.

3.4. Inference and Computational Analysis

Inference Pipeline. As illustrated in Figure 2, in each transformer block m , the gated selector first analyzes the input token sequence q_{m-1} and predicts the activation probability for each token. Based on this, it generates a binary indicator vector \mathcal{I} that identifies which tokens should be updated. Using the vector \mathcal{I} , a compact token subset \hat{q}_{m-1} is extracted from q_{m-1} and passed sequentially through the Attention and the expert-based FFN. Within the FFN, the dynamic router further assigns each token to the most suitable expert network according to the routing probabilities. After processing, the updated token representations \hat{q}_m are mapped

back to their original positions in the sequence using \mathcal{I} , resulting in the reconstructed output sequence q_m for block m . This output is then used as the input for the subsequent block in the generation process.

FLOPs Saving Analysis. We consider the computational costs of dynamic routers and gated selectors in FLOPs estimation. Let η denote the token saving rate, and μ denote the FFN weight saving rate. For a transformer block with input sequence length L and hidden dimension H , the FLOPs can be reduced by $8 \cdot \eta \cdot L \cdot H^2 \cdot (1 + 2\mu)$. Besides, the additional computational cost introduced by the dynamic gating and routing mechanisms is $2 \cdot L \cdot H \cdot (1 + N - \eta \cdot N)$, where N is the number of FFN expert networks. Therefore, the estimated FLOPs savings are computed as the difference between the reduction and the additional overhead:

$$\sum_{i \in \mathcal{S}} \sum_{j \in \mathcal{D}} [8 \cdot \eta_{i,j} \cdot L_{i,j} \cdot H^2 \cdot (1 + 2\mu_{i,j}) - 2 \cdot L_{i,j} \cdot H \cdot (1 + (1 - \eta_{i,j}) \cdot N)], \quad (12)$$

where \mathcal{S} denotes the set of steps that dynamically activate weight and token, and \mathcal{D} is the set of all transformer blocks.

4. Experiments

4.1. Experimental Setup

Models and Evaluation metrics. We implement ActVAR on multiple parameter-scale VAR models, including VAR-d16, VAR-d20, and VAR-d30, using the official pre-trained model’s parameters as initialization. All experiments are conducted on the ImageNet 256×256 conditional generation benchmark [28]. To ensure a fair comparison, we adopt the following evaluation metrics: Frechet Inception Distance (FID), Inception Score (IS), Precision, and Recall.

Implementation Details. We train the ActVAR models on the ImageNet-1K [28] dataset. The dynamic activation strategy for both FFN weights and tokens is applied during the generation steps of the final two scales. Specifically, the token and weight activation rates are set uniformly to

Type	Method	FLOPs Saving (%)	#Para	#Step	Fid (\downarrow)	IS (\uparrow)	Pre(\uparrow)	Rec (\uparrow)
Diff.	CDM	-	-	8100	4.88	158.7	-	-
	DiT-L/2	-	458M	250	5.02	167.2	0.75	0.57
	LDM-4-G	-	400M	250	3.60	247.7	-	-
AR	VQGAN-re	-	1.4B	256	5.20	280.3	-	-
	ViTVQ-re	-	1.7B	1024	3.04	227.4	-	-
	RQTran.-re	-	3.8B	68	3.80	323.7	-	-
VAR	VAR-d16	-	310M	10	3.30	274.4	0.84	0.51
	VAR-d20	-	600M	10	2.57	302.6	0.83	0.56
	VAR-d24	-	1.0B	10	2.09	312.9	0.82	0.59
	VAR-d30	-	2.0B	10	1.92	323.1	0.82	0.59
	ActVAR-d16	20.2%	310M	10	3.51	273.5	0.85	0.49
	ActVAR-d20	21.2%	600M	10	2.72	290.4	0.83	0.55
	ActVAR-d24	21.8%	1.0B	10	2.20	300.7	0.82	0.58
	ActVAR-d30	22.3%	2.0B	10	2.05	321.6	0.82	0.59

Table 1. Evaluation on the ImageNet 256x256 benchmark.

75% in these steps. Training is conducted in two phases. In the first phase, we train the dynamic router and the gated selector while freezing all other model parameters. In the second phase, the router and selector are kept fixed, while the expert FFNs, attention modules, and classification head are fine-tuned. For both phases, we adopt a batch size of 512 and a learning rate of $2e - 4$. The AdamW optimizer is employ with $\beta_1 = 0.9$, $\beta_2 = 0.95$, and a weight decay of 0.05. The training lasts for 2 epochs in the first phase and 10 epochs in the second.

4.2. Main Results

We compare ActVAR with state-of-the-art models, including VAR models [34], AR-based models [9, 17, 41], and Diffusion-based models [15, 23, 27], on the ImageNet 256×256 benchmark. The results, summarized in Table 1, demonstrate that ActVAR consistently achieves substantial computational savings across different model scales, with only marginal degradation in image quality. Specifically, ActVAR-d16 achieves a **20.2%** reduction in FLOPs, with only a 0.9 decrease in IS compared to VAR-d16. ActVAR-d24 reduces FLOPs by **21.8%**, while incurring only a 0.11 increase in FID compared to the similar-sized VAR-d24. Similarly, ActVAR-d30 maintains a **22.3%** reduction in FLOPs while preserving strong performance across all evaluation metrics. These results clearly indicate that ActVAR strikes an effective balance between efficiency and fidelity, substantially lowering computational overhead while maintaining the high generation quality characteristic of autoregressive models. Furthermore, ActVAR exhibits competitive results when compared to representative AR-based and Diffusion-based models.

We compare the images generated by VAR-d20 and ActVAR-d20, as illustrated in Figure 7. ActVAR-d20 delivers visual fidelity comparable to VAR-d20, showing no per-

Activation rates	FLOPs Saving (%)	FID (\downarrow)	IS (\uparrow)
(50%, 25%; 50%)	43.2%	3.30	256.8
(50%, 75%; 25%)	39.9%	3.21	265.1
(50%, 50%; 75%)	32.8%	2.92	274.1
(75%, 50%; 75%)	28.2%	2.89	277.1
(75%, 75%; 75%)	21.2%	2.72	290.4

Table 2. FLOPs saving and performance with varying activation ratios (α , β ; γ). Here, α and β denote the token activation ratios, and γ is the activated FFN weight ratio.

ceptible degradation while achieving a 21.2% reduction in FLOPs. This indicates that the dynamic expert and token selection mechanisms in ActVAR successfully allocate computation where it is needed, minimizing redundancy without sacrificing fidelity.

4.3. Ablation Studies

4.3.1. Activation Rates.

To validate the trade-offs between computational efficiency and model performance under varying activation rates, we compare different configurations of token and FFN activation ratios, as shown in Table 2. Lower activation rates (e.g., 50%, 25%; 50%) lead to greater FLOPs savings (up to 43.2%) but result in degraded generation quality, as reflected by higher FID and lower IS. In contrast, higher activation rates (e.g., 75%, 75%; 75%) reduce FLOPs savings but significantly improve performance. This shows the flexibility of ActVAR in supporting a wide range of efficiency-accuracy balance via simple adjustment of activation rates. In our study, we adopt the (75%, 75%; 75%) setting, which yields the best generation quality (FID 2.72, IS 290.4) while still saving 21.2% of FLOPs—demonstrating that high activation remains feasible with moderate efficiency gains when performance is prioritized.

Module	FLOPs Saving (%)	FID (\downarrow)	IS (\uparrow)
w/o DW	14.2%	2.67	290.5
w/o AT	9.4%	2.70	288.6
w/ DW & AT	21.2%	2.72	290.4

Table 3. **Ablation on the proposed components.** DW: Dynamic weight activation. AT: Adaptive token activation.

Module	FID (\downarrow)	IS (\uparrow)
Fixed token pruning	3.83	242.4
Dynamic activating token	2.72	290.4

Table 4. **Comparison of our dynamic token activation with fixed token pruning.**

4.3.2. The effectiveness of proposed components.

To evaluate the contribution of each component in ActVAR, we perform ablation studies on dynamic weight activation and adaptive token activation. The experimental results are summarized in Table 3. When either module is removed, the image generation quality tends to improve slightly. However, this comes at the cost of a substantial drop in FLOPs saving rates. For instance, removing dynamic weight activation increases the IS by 0.1, but decreases the FLOPs saving rate from 21.4% to 14.2%. Notably, excluding adaptive token activation leads to approximately a 50% reduction in FLOPs savings compared to the full ActVAR model, while the FID only decreases marginally by 0.02. These results demonstrate that both components are critical for maintaining a favorable trade-off between image generation quality and computational efficiency in ActVAR.

4.3.3. Analysis of dynamic token activation.

To analyze the advantages of dynamic token activation, we visualize the distribution of activated tokens across different blocks at a 16×16 spatial scale. As shown in Figure 6, the model exhibits diverse activation patterns: some blocks tend to focus on tokens associated with the background, while others prioritize tokens corresponding to foreground objects. This block-specific behavior highlights the adaptiveness of our proposed strategy, which effectively accommodates varying token preferences across spatial regions.

Moreover, our dynamic token activation enables broader token coverage. Since the sets of tokens activated by different blocks are not identical, their union covers a large portion of the input tokens. This ensures that most tokens can still participate in the update process, even under sparse activation constraints.

To further validate this behavior, we compare our token activation with a fixed token pruning baseline. For a fair comparison, both methods retain the same number of tokens. The key difference lies in adaptability: in fixed token pruning, once the token sequence is selected during the first step, it remains static throughout inference. In contrast, our

Method	FID (\downarrow)	IS (\uparrow)
Static weight pruning	3.04	274.2
Dynamic weight activation	2.72	290.4

Table 5. **Comparison of our dynamic weight activation with static weight pruning.**

method selects tokens adaptively for each block. Shown in Table 4, dynamic token activation achieves a lower FID and improves the IS by 48.0 points compared to fixed pruning. The results not only demonstrate the effectiveness of our method but also improve its interpretability by aligning token selection with block-level semantic preferences.

4.3.4. Analysis of Dynamic weight activation.

To verify the effectiveness of dynamic weight activation, we compare it with traditional static weight pruning. For fair comparison, both methods use the same weight activation rate and are trained under the same strategy. The results are shown in Table 5. Our dynamic method achieves better performance in both FID and IS. In particular, the IS of static pruning is 16.2 lower than our method, highlighting the advantage of dynamically adapting the computation pathway rather than permanently removing parameters. These results show that our approach can allocate weights more precisely for each token, achieving efficient and accurate computation.

Furthermore, Figure 5 illustrates that tokens at different steps display pronounced variations in their preferences for activated expert networks. This dynamic behavior confirms that our proposed mechanism effectively captures and adapts to these variations, enabling flexible computation while maintaining generation fidelity.

5. Conclusion

In this paper, we propose ActVAR, a dynamic and efficient framework for autoregressive image generation that addresses the computational challenges of next-scale prediction models like VAR. Unlike conventional static pruning approaches that permanently remove model components and risk degrading performance, ActVAR adopts a dynamic sparsity mechanism that selectively activates important computations based on the input content at each generation step. ActVAR consists of two core modules: a learnable expert router that dynamically allocates FFN sub-networks for each token, and a gated token selector that filters out less informative tokens to reduce attention overhead. This dual sparsity design concentrates computation on the most relevant regions, while a lightweight reconstruction module preserves global context and spatial alignment by reintegrating the skipped tokens.

Extensive experiments on the ImageNet 256×256 conditional generation benchmark demonstrate that Act-

VAR achieves up to 21.2% FLOPs reduction while maintaining competitive image quality, outperforming conventional static pruning methods. We believe ActVAR offers a promising direction for accelerating autoregressive generation models without sacrificing fidelity.

References

- [1] Sotiris Anagnostidis, Dario Pavlo, Luca Biggio, Lorenzo Noci, Aurelien Lucchi, and Thomas Hofmann. Dynamic context pruning for efficient and interpretable autoregressive transformers. *Advances in Neural Information Processing Systems*, 36:65202–65223, 2023. 3
- [2] Daniel Bolya, Cheng-Yang Fu, Xiaoliang Dai, Peizhao Zhang, Christoph Feichtenhofer, and Judy Hoffman. Token merging: Your vit but faster. *arXiv preprint arXiv:2210.09461*, 2022. 1
- [3] Tom Brown, Benjamin Mann, Nick Ryder, Melanie Subbiah, Jared D Kaplan, Prafulla Dhariwal, Arvind Neelakantan, Pranav Shyam, Girish Sastry, Amanda Askell, et al. Language models are few-shot learners. *Advances in neural information processing systems*, 33:1877–1901, 2020. 3
- [4] Jiajun Cao, Yuan Zhang, Tao Huang, Ming Lu, Qizhe Zhang, Ruichuan An, Ningning Ma, and Shanghang Zhang. Movekd: Knowledge distillation for vlms with mixture of visual encoders. In *Proceedings of the Computer Vision and Pattern Recognition Conference*, 2025. 2
- [5] Mark Chen, Alec Radford, Rewon Child, Jeffrey Wu, Heewoo Jun, David Luan, and Ilya Sutskever. Generative pre-training from pixels. In *International conference on machine learning*, pages 1691–1703. PMLR, 2020. 2
- [6] Xi Chen, Nikhil Mishra, Mostafa Rohaninejad, and Pieter Abbeel. Pixelsnail: An improved autoregressive generative model. In *International conference on machine learning*, pages 864–872. PMLR, 2018. 2
- [7] Jacob Devlin, Ming-Wei Chang, Kenton Lee, and Kristina Toutanova. Bert: Pre-training of deep bidirectional transformers for language understanding. In *Proceedings of the 2019 conference of the North American chapter of the association for computational linguistics: human language technologies, volume 1 (long and short papers)*, pages 4171–4186, 2019. 3
- [8] Alexey Dosovitskiy, Lucas Beyer, Alexander Kolesnikov, Dirk Weissenborn, Xiaohua Zhai, Thomas Unterthiner, Mostafa Dehghani, Matthias Minderer, Georg Heigold, Sylvain Gelly, et al. An image is worth 16x16 words: Transformers for image recognition at scale. *arXiv preprint arXiv:2010.11929*, 2020. 3
- [9] Patrick Esser, Robin Rombach, and Bjorn Ommer. Taming transformers for high-resolution image synthesis. In *Proceedings of the IEEE/CVF conference on computer vision and pattern recognition*, pages 12873–12883, 2021. 1, 3, 7
- [10] William Fedus, Barret Zoph, and Noam Shazeer. Switch transformers: Scaling to trillion parameter models with simple and efficient sparsity. *Journal of Machine Learning Research*, 23(120):1–39, 2022. 5, 1
- [11] Hang Guo, Yawei Li, Taolin Zhang, Jiangshan Wang, Tao Dai, Shu-Tao Xia, and Luca Benini. Fastvar: Linear visual autoregressive modeling via cached token pruning. *arXiv preprint arXiv:2503.23367*, 2025. 3
- [12] Jian Han, Jinlai Liu, Yi Jiang, Bin Yan, Yuqi Zhang, Zehuan Yuan, Bingyue Peng, and Xiaobing Liu. Infinity: Scaling bit-wise autoregressive modeling for high-resolution image synthesis. In *Proceedings of the Computer Vision and Pattern Recognition Conference*, pages 15733–15744, 2025. 1
- [13] Yefei He, Feng Chen, Yuanyu He, Shaoxuan He, Hong Zhou, Kaipeng Zhang, and Bohan Zhuang. Zipar: Accelerating auto-regressive image generation through spatial locality. *arXiv preprint arXiv:2412.04062*, 2024. 3
- [14] Geoffrey Hinton, Oriol Vinyals, and Jeff Dean. Distilling the knowledge in a neural network. *arXiv preprint arXiv:1503.02531*, 2015. 2, 4
- [15] Jonathan Ho, Chitwan Saharia, William Chan, David J Fleet, Mohammad Norouzi, and Tim Salimans. Cascaded diffusion models for high fidelity image generation. *Journal of Machine Learning Research*, 23(47):1–33, 2022. 7
- [16] Tao Huang, Shan You, Fei Wang, Chen Qian, and Chang Xu. Knowledge distillation from a stronger teacher. *Advances in Neural Information Processing Systems*, 35:33716–33727, 2022. 4
- [17] Doyup Lee, Chiheon Kim, Saehoon Kim, Minsu Cho, and Wook-Shin Han. Autoregressive image generation using residual quantization. In *Proceedings of the IEEE/CVF conference on computer vision and pattern recognition*, pages 11523–11532, 2022. 2, 7
- [18] Dmitry Lepikhin, HyukJoong Lee, Yuanzhong Xu, Dehao Chen, Orhan Firat, Yanping Huang, Maxim Krikun, Noam Shazeer, and Zhifeng Chen. Gshard: Scaling giant models with conditional computation and automatic sharding. *arXiv preprint arXiv:2006.16668*, 2020. 5, 1
- [19] Tianhong Li, Yonglong Tian, He Li, Mingyang Deng, and Kaiming He. Autoregressive image generation without vector quantization. *Advances in Neural Information Processing Systems*, 37:56424–56445, 2024. 3
- [20] Ze Liu, Yutong Lin, Yue Cao, Han Hu, Yixuan Wei, Zheng Zhang, Stephen Lin, and Baining Guo. Swin transformer: Hierarchical vision transformer using shifted windows. In *Proceedings of the IEEE/CVF international conference on computer vision*, pages 10012–10022, 2021. 3
- [21] Xinyin Ma, Gongfan Fang, and Xinchao Wang. Llm-pruner: On the structural pruning of large language models. *Advances in neural information processing systems*, 36:21702–21720, 2023. 3
- [22] Wael Mattar, Idan Levy, Nir Sharon, and Shai Dekel. Wavelets are all you need for autoregressive image generation. *arXiv preprint arXiv:2406.19997*, 2024. 3
- [23] William Peebles and Saining Xie. Scalable diffusion models with transformers. In *Proceedings of the IEEE/CVF international conference on computer vision*, pages 4195–4205, 2023. 3, 7
- [24] Dustin Podell, Zion English, Kyle Lacey, Andreas Blattmann, Tim Dockhorn, Jonas Müller, Joe Penna, and Robin Rombach. Sdxl: Improving latent diffusion mod-

- els for high-resolution image synthesis. *arXiv preprint arXiv:2307.01952*, 2023. 3
- [25] Aditya Ramesh, Mikhail Pavlov, Gabriel Goh, Scott Gray, Chelsea Voss, Alec Radford, Mark Chen, and Ilya Sutskever. Zero-shot text-to-image generation. In *International conference on machine learning*, pages 8821–8831. Pmlr, 2021. 1
- [26] Scott Reed, Aäron van den Oord, Nal Kalchbrenner, Victor Bapst, Matt Botvinick, and Nando De Freitas. Generating interpretable images with controllable structure. 2016. 2
- [27] Robin Rombach, Andreas Blattmann, Dominik Lorenz, Patrick Esser, and Björn Ommer. High-resolution image synthesis with latent diffusion models. In *Proceedings of the IEEE/CVF conference on computer vision and pattern recognition*, pages 10684–10695, 2022. 3, 7
- [28] Olga Russakovsky, Jia Deng, Hao Su, Jonathan Krause, Sanjeev Satheesh, Sean Ma, Zhiheng Huang, Andrej Karpathy, Aditya Khosla, Michael Bernstein, Alexander C. Berg, and Li Fei-Fei. ImageNet Large Scale Visual Recognition Challenge. *International Journal of Computer Vision (IJCV)*, 115 (3):211–252, 2015. 6
- [29] Tim Salimans, Andrej Karpathy, Xi Chen, and Diederik P Kingma. Pixelcnn++: Improving the pixelcnn with discretized logistic mixture likelihood and other modifications. *arXiv preprint arXiv:1701.05517*, 2017. 2
- [30] Michael Santacrose, Zixin Wen, Yelong Shen, and Yuanzhi Li. What matters in the structured pruning of generative language models? *arXiv preprint arXiv:2302.03773*, 2023. 3
- [31] Xuan Shen, Zhao Song, Yufa Zhou, Bo Chen, Jing Liu, Ruiyi Zhang, Ryan A Rossi, Hao Tan, Tong Yu, Xiang Chen, et al. Numerical pruning for efficient autoregressive models. In *Proceedings of the AAAI Conference on Artificial Intelligence*, pages 20418–20426, 2025. 3
- [32] Peize Sun, Yi Jiang, Shoufa Chen, Shilong Zhang, Bingyue Peng, Ping Luo, and Zehuan Yuan. Autoregressive model beats diffusion: Llama for scalable image generation. *arXiv preprint arXiv:2406.06525*, 2024. 1, 3
- [33] Haotian Tang, Yecheng Wu, Shang Yang, Enze Xie, Junsong Chen, Junyu Chen, Zhuoyang Zhang, Han Cai, Yao Lu, and Song Han. Hart: Efficient visual generation with hybrid autoregressive transformer. *arXiv preprint arXiv:2410.10812*, 2024. 1
- [34] Keyu Tian, Yi Jiang, Zehuan Yuan, Bingyue Peng, and Liwei Wang. Visual autoregressive modeling: Scalable image generation via next-scale prediction. *Advances in neural information processing systems*, 37:84839–84865, 2024. 1, 3, 7
- [35] Hugo Touvron, Matthieu Cord, Matthijs Douze, Francisco Massa, Alexandre Sablayrolles, and Hervé Jégou. Training data-efficient image transformers & distillation through attention. In *International conference on machine learning*, pages 10347–10357. PMLR, 2021. 3
- [36] Aaron Van den Oord, Nal Kalchbrenner, Lasse Espeholt, Oriol Vinyals, Alex Graves, et al. Conditional image generation with pixelcnn decoders. *Advances in neural information processing systems*, 29, 2016. 2
- [37] Aaron Van Den Oord, Oriol Vinyals, et al. Neural discrete representation learning. *Advances in neural information processing systems*, 30, 2017. 1, 3
- [38] Ashish Vaswani, Noam Shazeer, Niki Parmar, Jakob Uszkoreit, Llion Jones, Aidan N Gomez, Łukasz Kaiser, and Illia Polosukhin. Attention is all you need. *Advances in neural information processing systems*, 30, 2017. 3
- [39] Junke Wang, Yi Jiang, Zehuan Yuan, Bingyue Peng, Zuxuan Wu, and Yu-Gang Jiang. Omnitokenizer: A joint image-video tokenizer for visual generation. *Advances in Neural Information Processing Systems*, 37:28281–28295, 2024. 3
- [40] Rui Xie, Tianchen Zhao, Zhihang Yuan, Rui Wan, Wenxi Gao, Zhenhua Zhu, Xuefei Ning, and Yu Wang. Litevar: Compressing visual autoregressive modelling with efficient attention and quantization. *arXiv preprint arXiv:2411.17178*, 2024. 3
- [41] Jiahui Yu, Xin Li, Jing Yu Koh, Han Zhang, Ruoming Pang, James Qin, Alexander Ku, Yuanzhong Xu, Jason Baldridge, and Yonghui Wu. Vector-quantized image modeling with improved vqgan. *arXiv preprint arXiv:2110.04627*, 2021. 7
- [42] Lu Yu and Wei Xiang. X-pruner: explainable pruning for vision transformers. In *Proceedings of the IEEE/CVF conference on computer vision and pattern recognition*, pages 24355–24363, 2023. 3
- [43] Yuan Zhang, Chun-Kai Fan, Junpeng Ma, Wenzhao Zheng, Tao Huang, Kuan Cheng, Denis Gudovskiy, Tomoyuki Okuno, Yohei Nakata, Kurt Keutzer, et al. Sparsevlm: Visual token sparsification for efficient vision-language model inference. *International conference on machine learning*, 2024. 1
- [44] Yuan Zhang, Tao Huang, Jiaming Liu, Tao Jiang, Kuan Cheng, and Shanghang Zhang. Freekd: Knowledge distillation via semantic frequency prompt. In *Proceedings of the IEEE/CVF Conference on Computer Vision and Pattern Recognition*, pages 15931–15940, 2024. 4
- [45] Zhengyan Zhang, Yankai Lin, Zhiyuan Liu, Peng Li, Maosong Sun, and Jie Zhou. Moefication: Transformer feed-forward layers are mixtures of experts. *arXiv preprint arXiv:2110.01786*, 2021. 4
- [46] Zhongyu Zhao, Menghang Dong, Rongyu Zhang, Wenzhao Zheng, Yunpeng Zhang, Huanrui Yang, Dalong Du, Kurt Keutzer, and Shanghang Zhang. Factorllm: Factorizing knowledge via mixture of experts for large language models. *arXiv preprint arXiv:2408.11855*, 2024. 4
- [47] Chuanxia Zheng, Tung-Long Vuong, Jianfei Cai, and Dinh Phung. Movq: Modulating quantized vectors for high-fidelity image generation. *Advances in Neural Information Processing Systems*, 35:23412–23425, 2022. 2
- [48] Yanqi Zhou, Tao Lei, Hanxiao Liu, Nan Du, Yanping Huang, Vincent Zhao, Andrew M Dai, Quoc V Le, James Laudon, et al. Mixture-of-experts with expert choice routing. *Advances in Neural Information Processing Systems*, 2022. 2
- [49] Lei Zhu, Fangyun Wei, Yanye Lu, and Dong Chen. Scaling the codebook size of vq-gan to 100,000 with a utilization rate of 99%. *Advances in Neural Information Processing Systems*, 37:12612–12635, 2024. 3
- [50] Mingjian Zhu, Yehui Tang, and Kai Han. Vision transformer pruning. *arXiv preprint arXiv:2104.08500*, 2021. 3

ActVAR: Activating Mixtures of Weights and Tokens for Efficient Visual Autoregressive Generation

Supplementary Material

6. Details of two-stage training strategy

6.1. Stage 1: train the router and selector

Dynamic router. To train the routing module without direct supervision, we adopt a knowledge distillation approach. The original feedforward network serves as a teacher, while the expert networks act as student models. For each expert, we compute its mean squared error (MSE) with respect to the teacher’s output to obtain a distance vector $\{d_i^w\}_{i=1}^N$, reflecting how closely each expert approximates the teacher. We then select the top- k closest experts and apply a softmax to produce a pseudo-label matrix:

$$\mathcal{A}_w = \sigma(\text{top} - k(\{-d_i^w\}_{i=1}^N, K_w)), \quad (13)$$

which is used to supervise the routing probability p_w via a distillation loss:

$$L_{dis}^w = \text{KL}(p_w \parallel \sigma(\mathcal{A}_w)). \quad (14)$$

To prevent the router from overloading a few experts [10], we follow [18] and add a load balancing loss:

$$L_{bl}^w = \frac{K_w}{N} \sum_{i=1}^N \sum_{j=1}^{K_w} \mathbb{I}_j(x_i) R_j(x_i), \quad (15)$$

where $\mathbb{I}_j(x_i)$ indicates whether the j -th expert is selected for token x_i , and N is the number of expert networks.

Gated selector. We train the token selector using a strategy similar to the router. The full input sequence q_{m-1} is first processed by the transformer to produce an updated output q_m . We then compute the token-wise distance $\{d_i^t\}_{i=1}^M$ between q_{m-1} and q_m to estimate each token’s importance — tokens with larger changes are considered more informative. Based on these distances, we apply a top- k operation followed by softmax to generate a pseudo-label matrix:

$$\mathcal{A}_t = \sigma(\text{top} - k(\{d_i^t\}_{i=1}^M, K_t)), \quad (16)$$

which is used to supervise the selector via a Kullback–Leibler (KL) divergence loss:

$$L_{dis}^t = \text{KL}(p_t \parallel \sigma(\mathcal{A}_t)). \quad (17)$$

We also apply the same load balancing loss to encourage activation of different tokens:

$$L_{bl}^t = \frac{K_t}{L} \sum_{i=1}^N \sum_{j=1}^{K_t} \mathbb{I}_j(x_i) R_j(x_i). \quad (18)$$

where L is the length of the input sequence. Moreover, we retain the original classification loss L_{cls} from VAR to regularize the router and selector, promoting consistency with the final predictions of the teacher model.

Therefore, the final loss formula is expressed as:

$$L_{stage1} = L_{cls} + \sum_{i=1}^D (\alpha \cdot (L_{dis}^w + L_{dis}^t) + \beta \cdot (L_{bl}^w + L_{bl}^t)), \quad (19)$$

where α and β are loss weights, which are set to 0.05 and 0.01, respectively, and D denotes the number of transformer blocks.

6.2. Stage 2: fine-tune the expert FFNs

To fine-tune the expert network and other components of the student model, we apply both block-level and final output-level distillation schemes. This strategy enables the student model to adapt to the trained router and selector while effectively transferring knowledge from the teacher model.

For each transformer block, we utilize the MSE loss to align the hidden states of the student model with those of the teacher model:

$$L_b = \text{MSE}(q_m, \bar{q}_m), \quad (20)$$

where q_m and \bar{q}_m denote the output sequences of the student and teacher models at the m -th block, respectively.

In addition, we adopt the KL loss to align the output distributions of the student and teacher models:

$$L_f = \text{KL}(p \parallel \bar{p}), \quad (21)$$

where p and \bar{p} represent the predicted probability distributions of the student and teacher models, respectively.

The final loss for the second training stage is defined as:

$$L_{stage2} = L_{cls} + L_f + \frac{1}{D} \sum_{i=1}^D L_b, \quad (22)$$

where L_{cls} is the classification loss, and D denotes the number of transformer blocks.

7. More visual comparisons

To verify that ActVAR maintains high generated image quality on large-scale models, we conduct the visualization on ActVAR-d24 and ActVAR-d30. As shown in the Figure 8, ActVAR achieves high-quality image generation on large-scale models while reducing FLOPs by over 20%, demonstrating its effectiveness in balancing efficiency and quality.

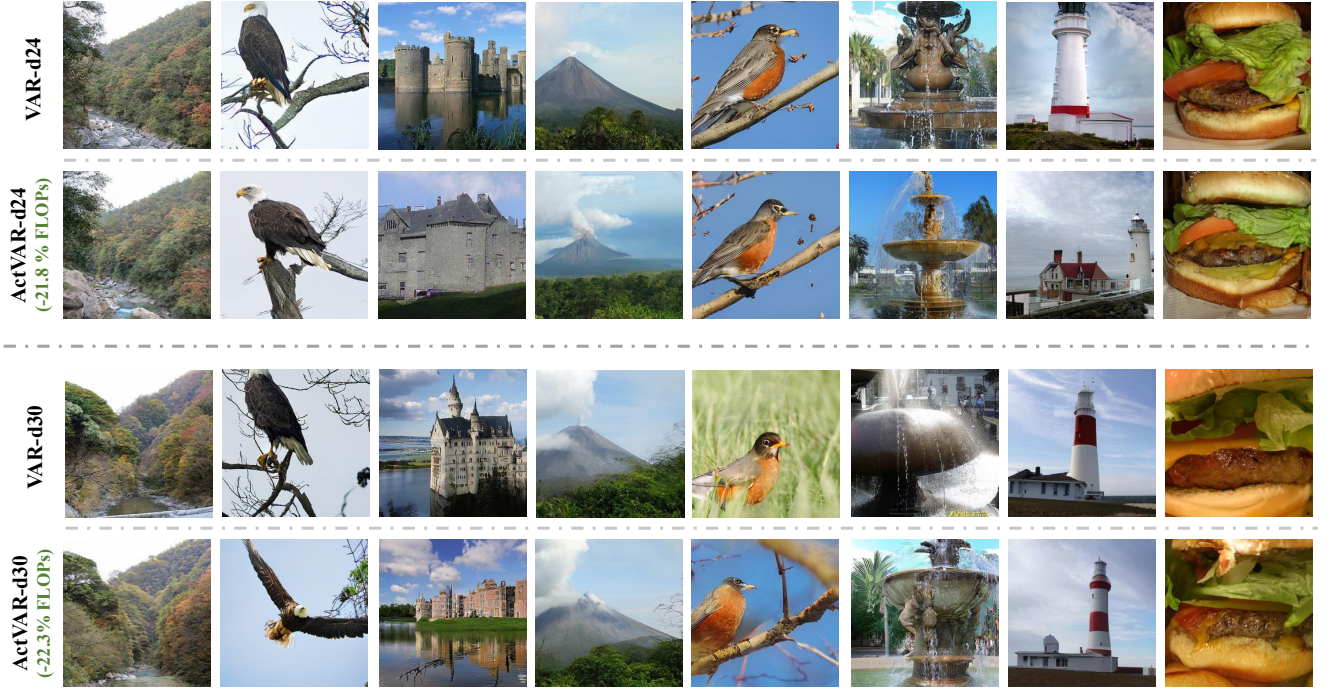


Figure 8. More visual comparisons on 256×256 image generation.

Activation scales	FLOPs Saving (%)	FID (↓)	IS (↑)
(7, 8)	8.1%	2.82	282.7
(9, 10)	21.2%	2.72	290.4

Table 6. FLOPs saving and performance at scales (ω , ρ). Here, ω and ρ represent the scales where ActVAR is employed.

8. Effects of ActVAR on different scales

In this work, ActVAR is applied at the last two scale steps (i.e., the 9th and 10th steps). We conduct an ablation study to validate this design choice by comparing it with an alternative setting where ActVAR is applied at earlier steps (i.e., the 7th and 8th steps), while keeping the token and weight activation rates consistent. As shown in Table 6, applying ActVAR in earlier steps results in more noticeable performance degradation. Moreover, since the token sequences are shorter in the earlier steps, the FLOPs saving achieved under the same activation rate is also limited. Therefore, applying ActVAR in the final two steps not only achieves more effective FLOPs savings but also better preserves generation quality.

9. Ablation on the number of expert networks

In this work, we decompose the original FFN into N expert networks. To explore the impact of this design, we con-

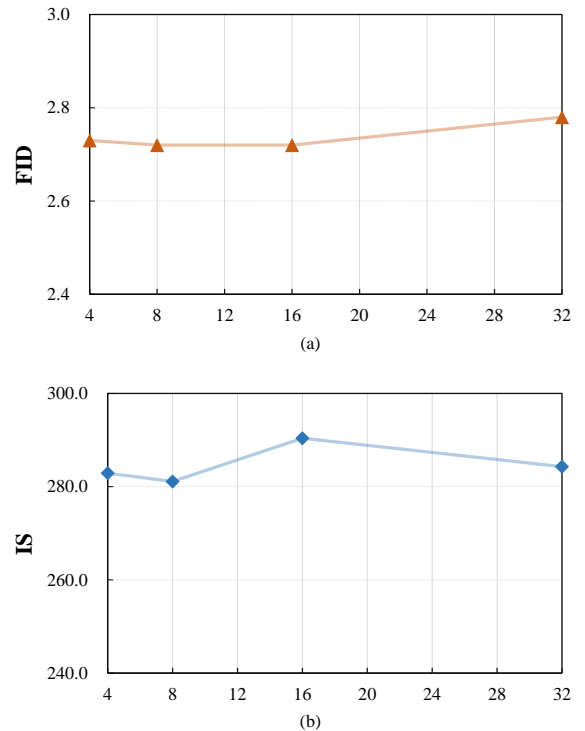


Figure 9. The impact of the number of experts on the generated image quality.

duct ablation studies on the number of experts. As shown in the Figure 9, setting a small number of experts (e.g., 4) leads to weaker performance. This is because coarse expert granularity limits the diversity of choices for input tokens. On the other hand, setting too many experts (e.g., 32) also degrades performance, as each expert has limited capacity and struggles to learn meaningful representations. Based on this trade-off, we set the number of experts to 16, which achieves an optimal balance between diversity and capacity, and yields the best performance.